ACS APPLIED MATERIALS & INTERFACES

Research Article

www.acsami.org

Dispersing Carbon Nanotubes by Chiral Network Surfactants

Pengcheng Lin, Yuehua Cong, and Baoyan Zhang*

Center for Molecular Science and Engineering, Northeastern University, Shenyang 110819, China

Supporting Information

ABSTRACT: Chiral network surfactants (CNSs) possessing miscibility with carbon nanotubes (CNTs) and chiral materials are applied to disperse CNTs. Ultraviolet−visible absorption spectroscopy is used to quantitatively determine the CNT concentration in homogeneous CNT−CNS dispersions, results indicate that CNSs with more mole fraction of polycyclic conjugated structure have better ability to load and disperse CNTs and the maximal concentration reaches 0.79 mg mL^{-1}. Fourier transform infrared imaging system is utilized to analyze the dispersibility of CNTs in CNT−CNS composites, and CNS with 6 mol % nonmesogens (S6) induces the best dispersibility. The CNT doped CNSs exhibit lower glass transition temperature, strengthened thermal stability, decreased the thermochromic temperature and enriched reflected colors of CNSs. Furthermore, S6 are used as a promoter to disperse CNTs in chiral host, here, a left-handed chiral liquid crystal (CLC) is selected, the miscibility between CNTs and CLCs is studied by polarized optical microscope, and CNTs can be effectively dispersed in CLCs by S6. The CNT dispersed CLCs can exhibit a faster electro-optical response process than neat CLCs.

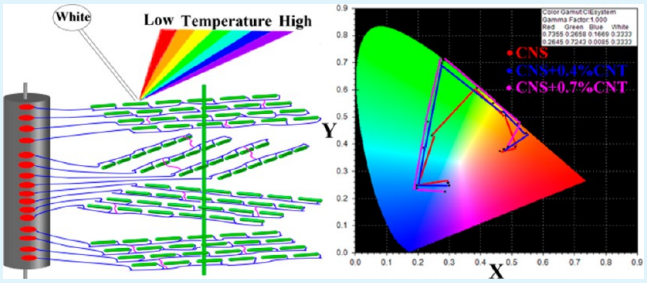

KEYWORDS: *dispersibility, carbon nanotubes, chiral network surfactants, thermal property, electro-optical response*

1. INTRODUCTION

Since the discovery by Iijima,[1] carbon nanotubes (CNTs) have make immense contributions to the rapid development of functional materials. CNTs have been used for high-performance electrochemical energy storage,[2,3] field emission display,[4] electronic devices,[5−7] biological detection,[8] and reinforced polymeric fibers.[9,10] However, pristine CNTs tend to form bundles because of strong intertube van der Waals binding energy,[11−14] and this makes the processing of CNTs become a practical challenge when exploiting their unique properties. To date, homogeneous CNT dispersions have been obtained by a large number of methods. Covalent bond functionalized CNTs can be evenly dispersed in organic solvents and polymers.[15] CNT dispersions also can be prepared by noncovalent modification using surfactants,[16,17] polymers,[18,19] and biological macromolecules.[20,21]

In addition to the above-mentioned methods, using thermotropic liquid crystals (LCs) to disperse CNTs is beneficial for both of them. The orientational behavior of CNTs can be preselected and determined through the self-ordering properties of LCs, and the orientational order parameter of CNTs reaches 0.9. Furthermore, CNTs can be reoriented by reorienting the LC director fields, this reorientation is due to the elastic interactions with anisotropic LC host.[22] Meanwhile, the physical properties of LCs can be enhanced by CNT doping. 1.5 wt % CNTs can improve the thermal stability of thermotropic liquid crystalline polymer as a result of the enhanced interfacial interactions between CNTs and polymer matrix.[23] The presence of 0.005 wt % CNTs in LCs can result in an increase in the dielectric anisotropy from 10.1 to 11.1, the reasons are mainly ascribe to the anchoring energy and anisotropic structure of CNTs.[24] The larger dielectric anisotropy of the high-aspect-ratio nanotubes and the parallel orientation of the nanotube to the LC director help reduce threshold voltage in the CNT-doped LCs.[25] The CNT doped LCs exhibit a faster relaxation process than neat LCs due to a reduced rotational viscosity.[26] It is worth mentioning that CNTs also can be dispersed in organic solvents with the assistance of surfactants, conjugated polymers or DNA, and the CNT dispersion can form a lyotropic LC system when the CNT concentration is high enough.[20,27,28] These studies provide a new way to process and align CNTs in the lyotropic liquid crystalline phase.

As nematic liquid crystals (NLCs) and CNTs share highly anisotropic molecular structure and properties, dispersing CNTs in NLCs has become a research hotspot in recent years.[29−34] The rod-shaped structure of CNTs enables them to tend to align along the director of NLCs. Meanwhile, in order to overcome the agglomerations of neighboring CNTs, polycyclic aromatic group pyrene is used to form $\pi-\pi$ stacking interaction with CNTs.[31]

In this Research Article, novel chiral network surfactants (CNSs) are designed and applied to disperse CNTs. The foundation of dispersing CNTs by CNSs is presented as following (see Schemes 1 and 2), the chiral mesogens on surfactants have compatibility with chiral liquid crystals (CLCs)

Received: January 7, 2015
Accepted: March 12, 2015
Published: March 19, 2015

DOI: 10.1021/acsami.5b00168
ACS Appl. Mater. Interfaces 2015, 7, 6724−6732

Scheme 1. Schematic Illustration of Dispersing CNTs by CNSs[a])

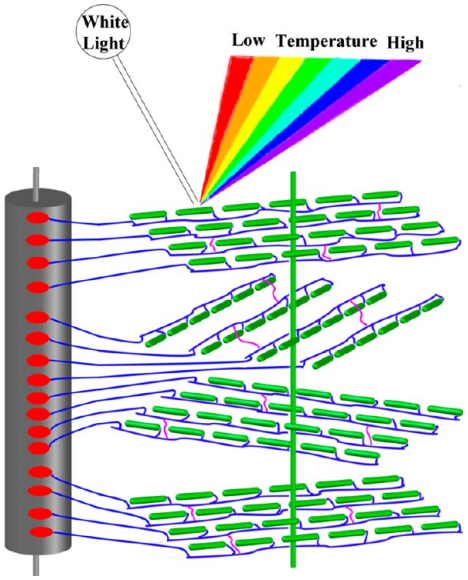

[a]The gray and green lines represent the parallel chiral axis of CNT and CNS. The backbone of CNSs (blue), chiral mesogens (green rods), crosslinking units (pink), and polycyclic conjugated structure in nonmesogens (red) are listed. The dispersed CNTs can improve the thermochromic properties of CNSs (described in the section 3.5).

by joining the helical matrix of CLC, polycyclic conjugated structure in nonmesogens are supposed to anchor on CNT surface by π-stacking, and cross-linking network is involved in the structure of surfactant to endow the dispersion system with more stability.

2. EXPERIMENTAL SECTION

2.1. Materials. The multiwalled CNTs synthesized by a chemical vapor deposition method were obtained from Shenzhen nano harbor, purity of the pristine CNTs was 95 wt %, diameter ranged from 2 to 5 nm and the length was between 0.5 and 2 μm. The CLC L581 was supplied by Shijiazhuang Chengzhi Yonghua Display Materials Co, Ltd., which was a left-handed material with a clearing point (T_c) of 88.2 °C. The polarized optical textures of CLC L581 were shown in Supporting Information Figure S1.

2.2. CNS Synthesis. The chemical structure of novel CNSs was presented in Scheme 2. The synthesis procedure of CNSs was described in Supporting Information. Key parameters of synthesized CNSs were summarized in Table 1.

2.3. Preparation of Homogenous CNT−CNS Dispersions. Six CNS−chloroform solutions were obtained by mixing 40 mg of accurately weighed CNS (S1−S6) with 5 mL of chloroform in six sample bottles. Six CNT−CNS suspensions were prepared by dissolving 10 mg of CNTs into the above-mentioned six CNS−chloroform solutions. To achieve homogeneous CNT−CNS dispersions, six suspensions were sonicated and centrifuged at a speed of 4000g for 30 min. The sonication parameter settings were kept the same throughout the whole article: temperature held at 25 °C, ultrasonic power at 100 W, an amplitude at 50%, in a deionized water bath and time for 30 min.

Scheme 2. Chemical Structure of CNSs[a]

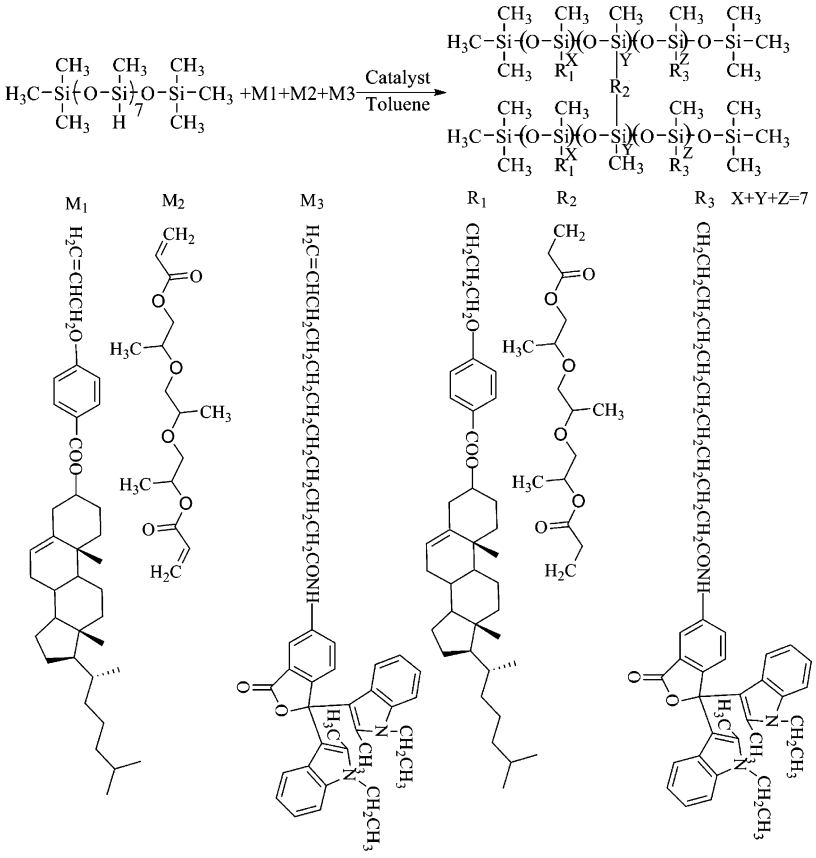

[a]R1 is chiral mesogen; R2 is flexible crosslinking unit, and R3 is nonmesogen with long hydrocarbon chain and polycyclic conjugated structure.

DOI: 10.1021/acsami.5b00168
ACS Appl. Mater. Interfaces 2015, 7, 6724−6732

Table 1. Polymerization, Specific Rotation ($[\alpha]_D^{20}$), Glass Transition Temperature (T_g), and T_c of CNSs

samples	PMHS (mmol)	M1 (mmol)	M2 (mmol)	M3 (mmol)	M3 (mol %)	T_g (°C)	T_c (°C)	$[\alpha]_D^{20}$
S1	0.471	2.700	0.3	0.000	0.0	47.11	185.8	−11.28
S2	0.471	2.694	0.3	0.006	0.2	45.42	184.5	−11.23
S3	0.471	2.688	0.3	0.012	0.4	44.46	183.4	−11.15
S4	0.471	2.682	0.3	0.018	0.6	41.97	182.6	−11.05
S5	0.471	2.676	0.3	0.024	0.8	40.38	180.8	−10.94
S6	0.471	2.670	0.3	0.030	1.0	37.00	179.7	−10.81

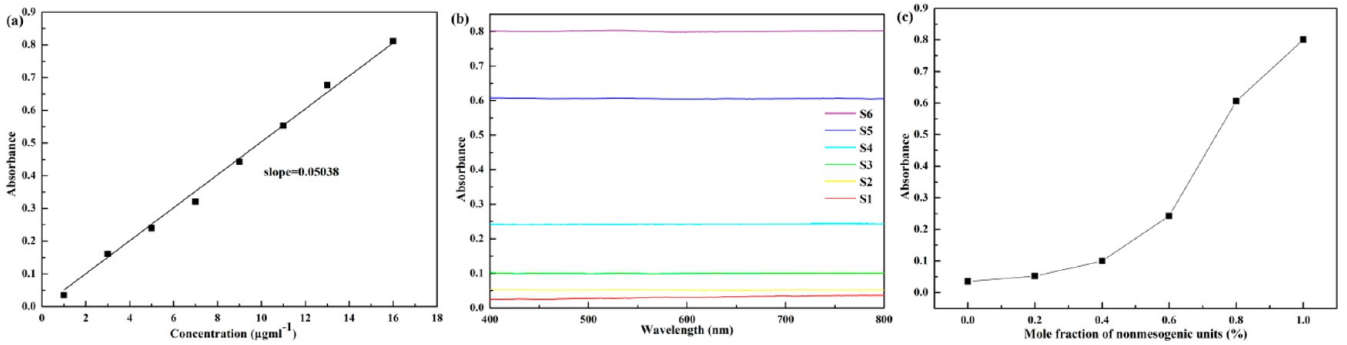

Figure 1. (a) Calibration plot of CNTs at 700 nm. (b) UV−vis absorption spectra of diluted CNT−CNS dispersions. (c) Optical absorbance values at 700 nm versus mole fraction of nonmesogens on CNSs.

2.4. Preparation of CNT−CNS Composites. Six CNT−CNS composites were prepared in the following way: six homogeneous CNT−CNS dispersions were vacuum-dried in an oven at 50 °C to remove chloroform.

2.5. Preparation of CLC−CNT-S6 Composites. An appropriate volume of CNT-S6 (0.79:8 wt/wt described in section 3.1) dispersion (prepared in section 2.3) was mixed with CLC L581 and followed by sonication. The mixture was vacuum-dried at 50 °C to remove chloroform. By setting the proportion of CLC and CNT-S6 dispersion, composites with different proportions of CLC, CNT, and S6 were prepared.

2.6. Instruments and Characterization. *2.6.1. Specific Rotation.* The specific rotation values of CNSs were measured by PerkinElmer 341 polarimeter (D line of a sodium vapor lamp, 589 nm) in chloroform at 20 °C.

2.6.2. Ultraviolet−Visible−Near Infrared (UV−vis−NIR) Absorption Spectroscopy. UV−vis−NIR spectrometer (PerkinElmer, lambda 950) was used to detect the CNT concentration in homogeneous CNT−CNS dispersion as follows: The UV−vis spectra data of eight CNT−chloroform solutions (concentrations ranging from 1 to 16 μg mL^{-1}) were collected after sonicated, and a calibration plot was made by monitoring the absorbance at 700 nm as a function of the CNT concentration. Subsequently, to make sure that the detected CNT concentration was within the in the linear range of calibration plot, CNT−CNS dispersion was diluted 50 times. Meanwhile, a diluted CNS solution was prepared by dissolving 40 mg of CNS in 5 mL of chloroform and diluting 50 times, the diluted CNT−CNS dispersion was added into the sample quartz cuvette (10 mm width), the diluted CNS solution was added into the reference quartz cuvette (10 mm width). Then, the unknown CNT concentration in dispersion was able to be determined by measuring its optical absorbance.

2.6.3. Fourier Transform Infrared (FTIR) Imaging. FTIR imaging system (PerkinElmer, Spectrum spotlight 300) provides two modes to evaluate the distribution of single component in multicomponents, transmission mode, and attenuated total reflectance (ATR) mode. Transmission mode collects the overall information about samples, including surface information and inner information, ATR mainly collect the surface information on thin films. In this work, transmission mode was selected to characterize the dispersibility of CNTs in CNT−CNS composites. Liquid nitrogen was used to make sure the temperature of IR detector is at 70 K.

2.6.4. Differential Scanning Calorimetry (DSC). The thermal phase transition behavior of CNSs and CNT−CNS composites was characterized using DSC (Q2000, TA Instruments, New Castle). The samples were heated at 10 °C min^{-1} in a nitrogen environment with a nitrogen gas flow rate of 50 mL min^{-1}.

2.6.5. Thermogravimetric Analysis (TGA). TGA was performed in nitrogen with a NETZSCH TG 209C instrument at a heating rate of 10 °C min^{-1} to probe the thermal stability of S6 and CNT embedded S6.

2.6.6. Microscope Camera. The reflected images in the section of Bragg selective reflection were taken by ProgRes microscope camera (JENOPTIK).

2.6.7. Polarized Optical Microscope (POM). Polarized optical textures of CNSs and CLC−CNT−S6 composites were observed by a Carl Zeiss Scope A1 instrument. The samples were heated and cooled at 1 °C min^{-1} with a Linkam heating and cooling stage.

2.6.8. Liquid Crystal Display (LCD) Tester. The electro-optical response measurements of CLCs and CLC−CNT−S6 composites were conducted using a LCD tester (North LCD Engineering Center). The cells were made from glass substrates, containing patterned ITO electrodes and planar aligning polyimide layer, the cell gap was maintained by 5 μm spacers. The frequency of applied square-wave voltage is 1000 Hz.

3. RESULTS AND DISCUSSION

3.1. Determination of Dispersed CNT Concentration. Chloroform was selected as solvent in the UV−vis experiment because of lack of chromophores (C═C, C≡C, C═O, N═N, and benzene) and auxochromes (−OH, −NH, −O−, and −SH). Therefore, solvent effects were avoided in the detection process. The UV−vis spectra of diluted CNT−CNS dispersions are presented in Figure 1b, and the corresponding absorbance values at 700 nm are listed in Figure 1c. With the linear calibration plot (see Figure 1a) in hand, we are able to calculate the original CNT concentrations in CNT−CNS dispersions, they are estimated to be 0.035, 0.051, 0.099, 0.024, 0.60, and 0.79 mg mL^{-1}, respectively. This result indicates CNSs with more mole fraction of polycyclic conjugated structure have better ability to load and disperse CNTs.

DOI: 10.1021/acsami.5b00168
ACS Appl. Mater. Interfaces 2015, 7, 6724−6732

3.2. Dispersibility of CNTs in CNT−CNS Composites. The IR absorption spectra of CNSs and raw CNTs are listed in Figure 2, CNTs exhibit distinct absorptions at 772 and 1219 cm^{-1}, CNSs exhibit strong absorptions at 772 and 1714 cm^{-1}. Subsequently, the total IR absorption of CNT−CNS composites was tested by FTIR imaging transmission mode. Finally, the exclusive IR absorption of CNSs at 1714 cm^{-1} was marked in the total absorption of CNT−CNS composites to analyze the miscibility between CNTs and CNSs. The FTIR images of CNT−CNS composites are displayed in Figure 2a−d, the green areas represent weaker absorption at 1714 cm^{-1}, the yellow and red areas represent stronger absorption at 1714 cm^{-1}. As 1714 cm^{-1} is the exclusive IR absorption peak of CNSs, it indicates CNSs mainly exist in the yellow and red areas. The relatively large and contiguous yellow areas in Figure 2a suggest that only few CNTs are dispersed in CNS matrix. The yellow areas in Figure 2d are more scattered than those in Figure 2a, indicating that there are more CNTs being loaded and dispersed by CNS matrix (see Scheme 1), meanwhile, yellow areas in Figure 2d present an uniform distribution, which proves the dispersibility of CNTs in CNT−CNS composites is excellent. On the basis of the above analysis, we conclude that S6 is the best dispersant among S1−S6.

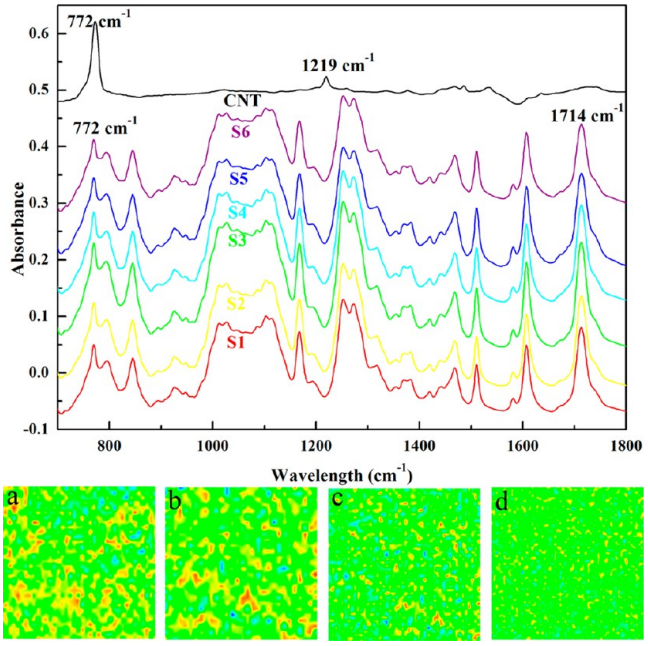

Figure 2. FTIR spectra of CNTs and CNSs (S1−S6) and FTIR images of composite CNT-S1 (a), CNT-S2 (b), CNT-S4 (c), and CNT-S6 (d).

3.3. Thermal Phase Transition. T_g is connected with the chain stiffness, chain length, chain movement, and free volume of oriented polymers. Thermal phase transition analysis can be used to figure out T_g. As shown in Figure 3a (solid lines), all the CNSs possess obvious glass transition with T_g ranging from 47.11 to 37 °C. To examine the effect of the dispersed CNTs on T_g of CNSs, the thermal phase transition of six CNT−CNS composites are summarized in Figure 3a (dash lines). On the basis of the information in Figure 3b, we can see CNT dispersed CNSs show lower T_g than neat CNSs, the reason for the decreased T_g of CNSs in the presence of CNTs is as follows: without doped CNTs, the nonmesogens on CNSs tend to join the spiral liquid crystalline matrix, which is constructed by the chiral mesogens on CNSs, and become a part of the matrix, this is the so-called guest−host effect. As liquid crystalline matrix is an ordered and stable structure, it is relatively difficult for segments in matrix to move. When CNTs are embedded in the CNSs matrix, on one hand, CNTs will bring an external disturbance to the original spiral liquid crystalline matrix. On the other hand, the nonmesogens on CNSs unite with CNTs and are not confined to the ordered and stable CNS matrix. There is more space and larger degree of freedom for segments in CNS matrix to move. Meanwhile, Figure 3a shows there are no additional phase-separated peaks for CNT−CNS composites, indicating that the dispersed CNTs do not give rise to phase separation in CNS matrix.

3.4. Thermal Stability. The thermal stability of polymers which is related to molecular structure and molecular weight is important to estimate their working temperature limits. The 2 wt % CNT embedded S6 and 4 wt % CNT embedded S6 were prepared according to a similar procedure which is described in sections 2.3 and 2.3. The TGA curves of raw CNT, S6, 2 wt % CNT embedded S6, and 4 wt % CNT embedded S6 in nitrogen are shown in Figure 4a. The results reveal that raw

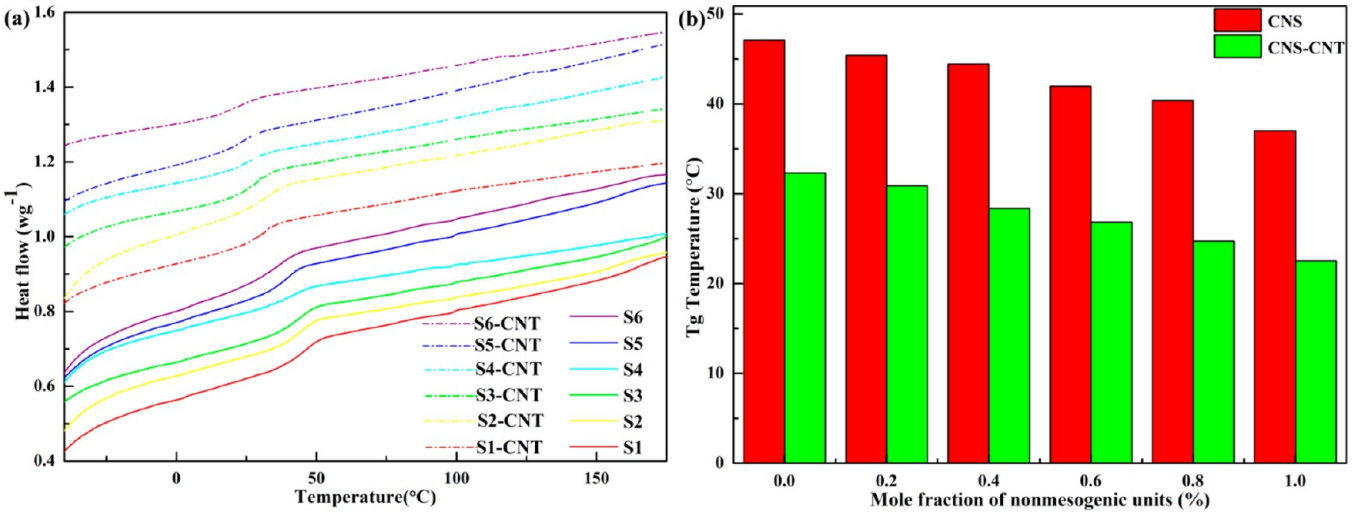

Figure 3. (a) DSC thermograms of CNSs and CNT−CNS composites. (b) T_g of CNSs and CNT−CNS composites.

DOI: 10.1021/acsami.5b00168
ACS Appl. Mater. Interfaces 2015, 7, 6724−6732

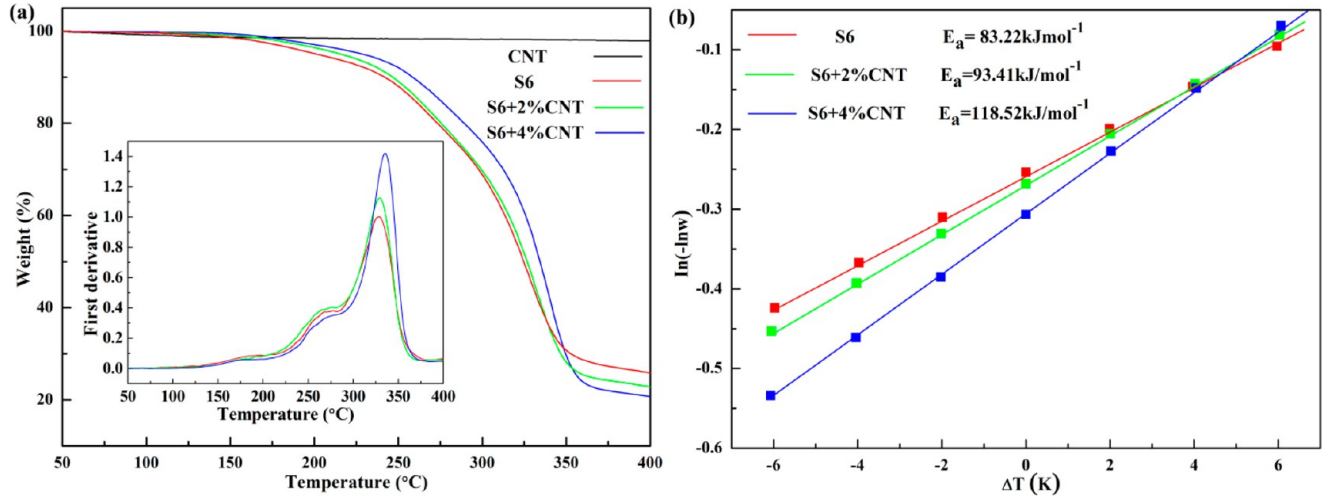

Figure 4. (a) TGA thermographs and corresponding first derivatives of raw CNT, S6, 2 wt % CNT embedded S6, and 4 wt % CNT embedded S6. (b) The plots of ln(-ln w) versus ΔT for S6, 2 wt % CNT embedded S6, and 4 wt % CNT embedded S6.

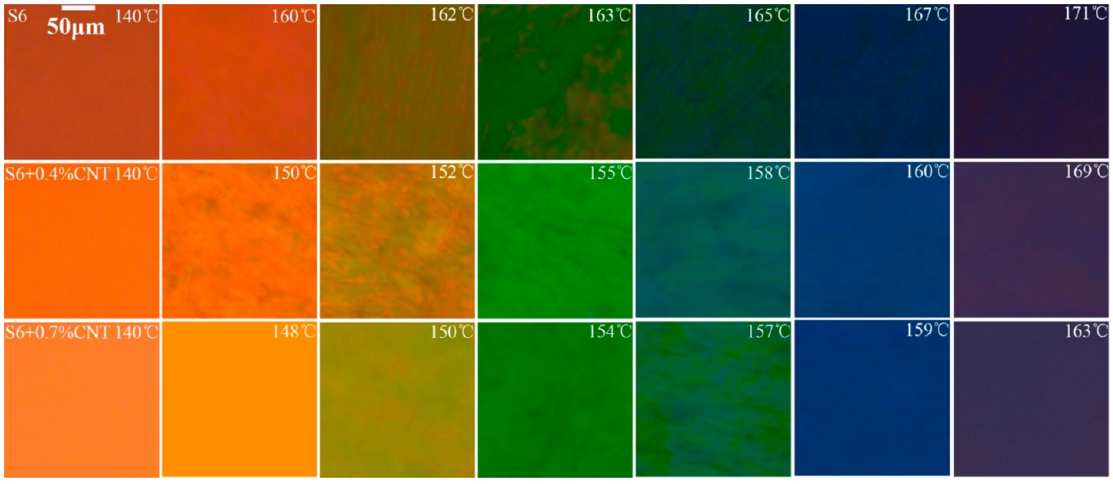

Figure 5. Reflected images of S6, S6 + 0.4 wt %CNT, and S6 + 0.7 wt %CNT.

CNTs are thermally stable within the temperature range 50−400 °C. The temperatures at 5% weight loss (decomposition temperatures) of S6, 2 wt % CNT embedded S6 and 4 wt % CNT embedded S6 are 201.30 °C, 216.13 and 228.29 °C, the reason for the increased decomposition temperatures of S6 in the presence of CNTs is mainly ascribe to the excellent thermal stability of CNTs and the interaction between CNS matrix and CNTs.[35]

The peaks in the first derivatives of S6, 2 wt % CNT embedded S6 and 4 wt % CNT embedded S6, show that three samples share almost the same temperatures at maximum decomposition rate (T_{rm}), it is implied that the thermal decomposition behavior of three samples mainly stems from their CNS matrix. Horowits−Metzger integral kinetic method is applied to further examine the decomposition process.[36]

$$\ln(-\ln w) = \frac{E_a \Delta T}{R T_{rm}^2} + k \quad (1)$$

where ΔT is defined as $\Delta T = T - T_{rm}$, E_a is activation energy of thermal decomposition, R is universal gas constant, k is the intercept of linear equation, and w is residual weight percentage. On the basis of the slope of the plot of ln(−ln w) versus ΔT(see Figure 4b), the E_a of S6, 2 wt % CNT embedded S6, and 4 wt % CNT embedded S6 are estimated to be 83.96, 93.41, and 118.52 kJ mol^{-1}, and the increased E_a can be attributed to the stable thermal stability of CNTs. Meanwhile, the increased E_a values are also consistent with the increased decomposition temperatures, this phenomenon proves that the evenly dispersed CNTs can enhance the thermal stability of S6.

3.5. Bragg Selective Reflection. A CLC can be regarded as a self-assembled one-dimensional photonic crystal.[37] Selective reflection of circularly polarized light according to Bragg's law is the most important optical property of CLCs, and the reflection wavelength (λ) can be determined from eq 2,[38−40] where $\bar{n}$ is the average refractive index of the LC medium, P is defined as the distance over which the director of CLC rotates by a full 360°. If P coincides with the wavelength of visible light, CLCs will reflect a brilliant color.

$$\lambda = \bar{n} \quad (2)$$

To study the effect of CNTs on the Bragg selective reflection of CNSs, the reflected image of S6, S6 + 0.4 wt %CNT, and S6 + 0.7 wt %CNT were observed, the detailed preparation of S6-CNT composites was similar to section 2.3 and 2.4. Two conclusions can be drawn from Figure 5, first, all the samples exhibit thermochromic property, and the reflected color is

DOI: 10.1021/acsami.5b00168
ACS Appl. Mater. Interfaces 2015, 7, 6724−6732

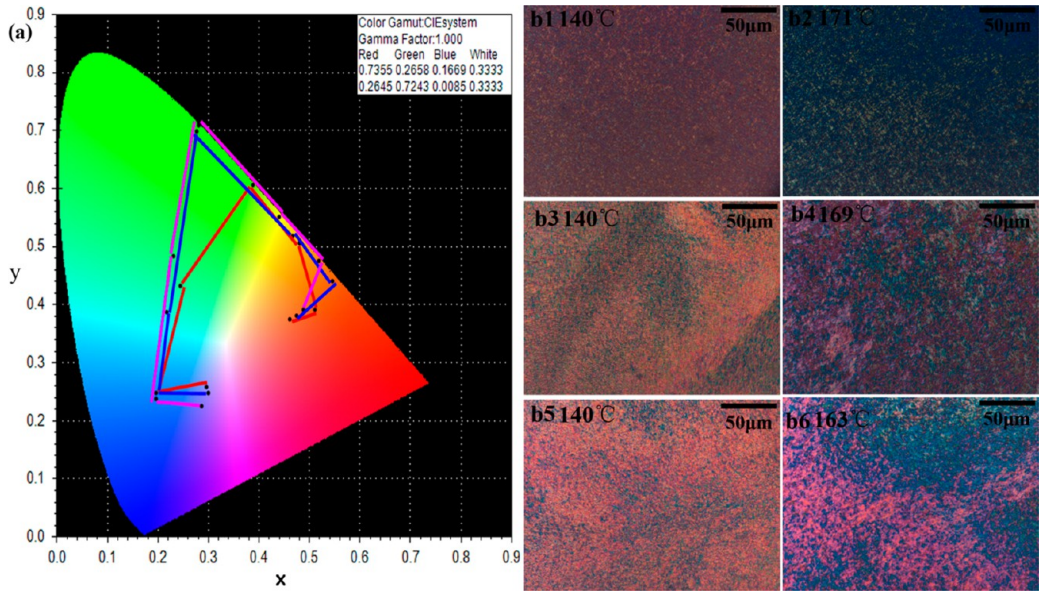

Figure 6. (a) Chromaticity diagrams of reflected images of S6 (red), S6 + 0.4 wt %CNT (blue), and S6 + 0.7 wt %CNT (pink). Optical textures of S6 (b1, b2), S6 + 0.4 wt %CNT (b3, b4), and S6 + 0.7 wt %CNT (b5, b6), crossed polarizers, 200×.

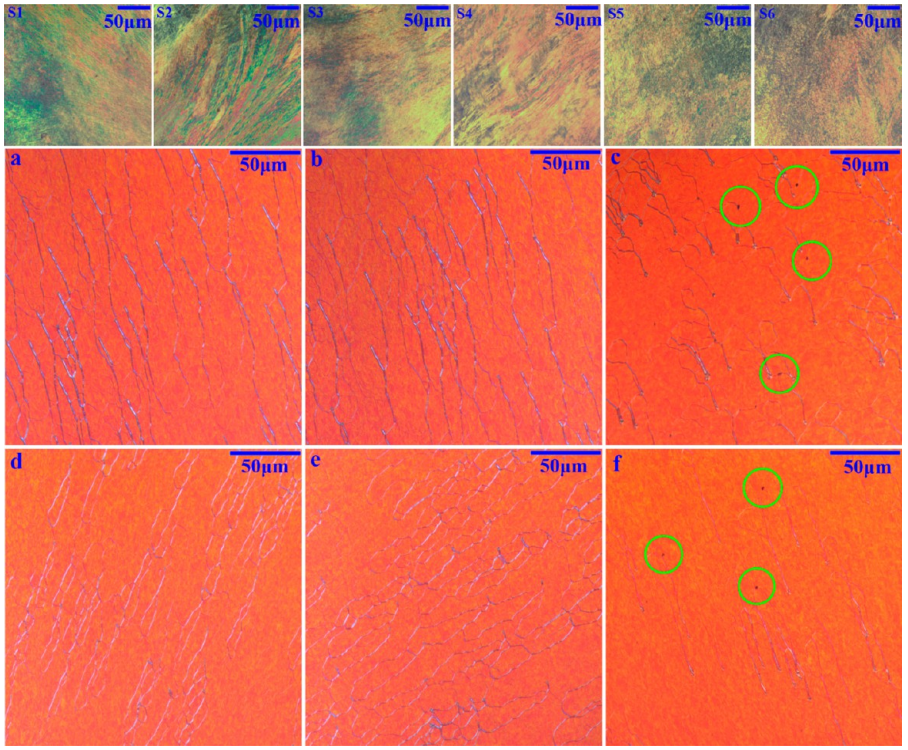

Figure 7. Polarized optical textures of CNSs (S1−S6) at 120 °C, and polarized optical textures of CLC (a), CLC+0 wt %CNT+1 wt %S6 (b), CLC +0.06 wt %CNT+0 wt %S6 (c), CLC+0.03 wt %CNT+0.31 wt %S6 (d), CLC+0.06 wt %CNT+0.62 wt %S6 (e), and CLC+0.09 wt %CNT+0.93 wt %S6 (f) at 25 °C, the aggregations of CNTs are delineated by green circles (crossed polarizers, 200×).

changing from orange to purple with the increase of temperature, this phenomenon can be explained by the following reason, within the discussed temperature range, all the samples show grandjean textures (see Figure 6b1−b6), which indicates that all the samples in Figure 5 are CLCs and the P of CLCs decreases as temperature increases, so the λ of reflection light became smaller according to eq 2. Meanwhile, the thermochromic temperature ranges of S6 + 0.4 wt %CNT and S6 + 0.7 wt %CNT are 140−169 and 140−163 °C, which are lower than that of neat S6 (140−171 °C); this can be explained by the following mechanism: the evenly dispersed CNTs are embedded in the CNS matrix (see Scheme 1), and the embedded CNTs bring their anisotropic thermal conductivity to the helical matrix of CNSs, which make CNSs more sensitive to the increased temperature to change their helical structure.

Furthermore, a chromaticity diagram was obtained by converting the RGB values of the reflected images in Figure

DOI: 10.1021/acsami.5b00168
ACS Appl. Mater. Interfaces 2015, 7, 6724−6732

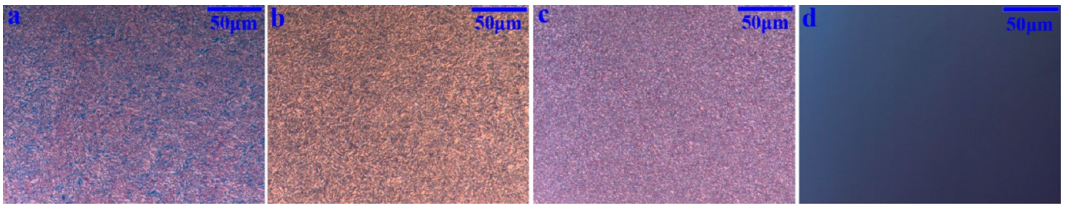

Figure 8. Polarized optical textures of CLC+0.06 wt %CNT+0.62 wt %S6 composites under electric fields, a (5v), b (15v), c (25v), and d (40v).

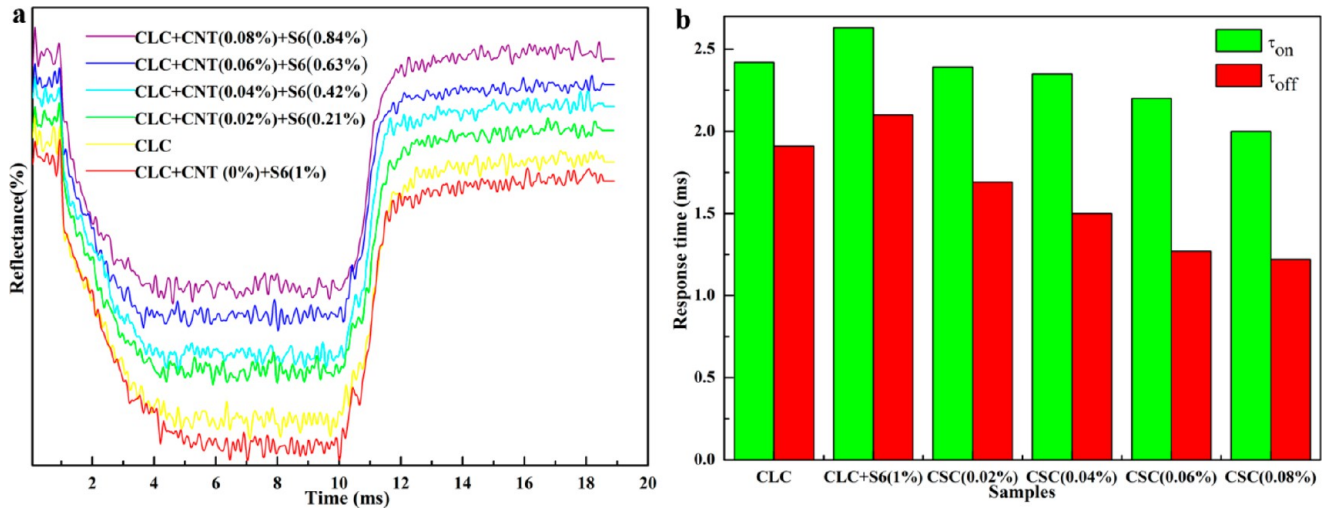

Figure 9. (a) Electro-optical response curves of reflectance versus time. (b) τ_{on} and τ_{off} of CLC, CLC+0 wt %CNT+1 wt %S6 (CLC+S6), CLC+0.02 wt %CNT+0.21 wt %S6 (CSC0.02%), CLC+0.04 wt % CNT+0.42 wt % S6 (CSC0.04%), CLC+0.06 wt %CNT+0.63 wt %S6 (CSC0.06%), and CLC+0.08 wt % CNT+0.84 wt %S6 (CSC0.08%) at 25 °C.

5 to chromaticity coordinates (see Figure 6), the detailed converting process was listed in Supporting Information. The areas confined by the chromaticity coordinates of S6 + 0.4 wt % CNT and S6 + 0.7 wt %CNT are larger than that of neat S6, indicating that the addition of CNTs can enrich the reflected colors of S6 when increasing the temperature, this result can be explained by the following analysis, if the P of CLC is heterogeneous at a certain temperature, and the λ of reflection light will be heterogeneous according to eq 1, which makes the chromaticity coordinates and the area confined by the chromaticity coordinates of the reflected image close to (0.33, 0.33). Therefore, the relatively long distance between the chromaticity coordinates and (0.33, 0.33) and the relatively large area confined by the chromaticity coordinates in Figure 6 are caused by the relatively uniform P of CNSs.

3.6. POM Texture. The existence of liquid crystal phases and polarized optical textures of LCs can be detected by POM. As shown in Figure 7, CNSs (S1−S6) display grandjean textures of chiral nematic phase. Meanwhile, the polarized optical textures of CNSs tend to be more gray from S1 to S6, suggesting that the liquid crystalline behavior of CNS becomes less obvious with the increase of mole fraction of nonmesogens on CNS.

To apply CNSs to disperse CNTs in chiral host and to improve the compatibility between CNTs and chiral host, a ternary system was established by CNTs, S6 and CLC L581. Samples involved in this section were CLC, CLC+0 wt %CNT +1 wt %S6, CLC+0.06 wt %CNT+0 wt %S6, CLC+0.03 wt % CNT+0.31 wt %S6, CLC+0.06 wt %CNT+0.62 wt %S6, and CLC+0.09 wt %CNT+0.93 wt % S6. The microstructure and dispersion state of CLCs and CLC−CNT-S6 composite were studied using POM. CLC and CLC+0 wt %CNT+1 wt %S6 share the same planar oily streak textures (see Figure 7a and b), indicating that S6 possesses good compatibility with CLC. There are aggregations of CNTs in the composite of CLC+0.06 wt %CNT+0 wt %S6 as a result of the strong $\pi-\pi$ stacking interaction between neighboring CNTs. However, 0.03 wt % CNTs and 0.06 wt % CNTs can be evenly dispersed in CLCs without formation of aggregations (see Figure 7d and e), which proves CNTs have excellent compatibility with CLCs with assistance of surfactant S6. On one hand, the chiral mesogens on S6 have compatibility with CLCs by joining the helical matrix of CLCs. On the other hand, the polycyclic conjugated structure in nonmesogens possesses affinity for CNTs. It is worth mentioning that there is side effect in the composite of CLC+0.09 wt %CNT+0.93 wt %S6 (see Figure 7f) because of the limited dispersing ability of S6. Meanwhile, the polarized optical textures of CLC+0.06 wt %CNT+0.62 wt %S6 composite indicate there is no aggregation of CNTs under electric fields (see Figure 8), proving that S6 maintains the dispersibility of CNTs in LC host under electric fields.

3.7. Electro-Optical Response. In the field of LC display, CNTs can be used to improve the performances of LCs in the process of Fréedericksz transition by increasing dielectric anisotropy, decreasing threshold voltage and accelerating electro optical response. To study the effect of dispersed CNT on the electro-optical response of CLCs, four CLC−CNT−S6 composites were prepared, CLC+0.02 wt %CNT +0.21 wt %S6 (CSC0.02%), CLC+0.04 wt %CNT+0.42 wt % S6 (CSC0.04%), CLC+0.06 wt %CNT+0.63 wt %S6 (CSC0.06%), and CLC+0.08 wt %CNT+0.84 wt %S6 (CSC0.08%), respectively, CLC and CLC+0 wt %CNT+1 wt %S6 (CLC+S6) were studied as reference samples.

DOI: 10.1021/acsami.5b00168
ACS Appl. Mater. Interfaces 2015, 7, 6724−6732

The electro-optical response curves are shown in Figure 9a, the field-on response time τ_{on} and field-off response time τ_{off} are illustrated in Figure 9b. First, the response times of CLC+CNT +S6 composites decline obviously with the increase of CNT concentration. This can be attributed to the following mechanism, more CNTs dispersed in LCs lead to lower rotational viscosity of LCs,[26] and the decreased rotational viscosity can help LC make a faster response to the electric field.[41] Second, τ_{on} is longer than τ_{off} for all samples, the differences in on and off times are due to the different driving forces, dielectric torque in the former, elastic deformation in the latter. Lastly, we note that the response time of CLC+S6 composites is longer than that of neat CLCs, this is because higher viscosity of S6 makes it difficult for CLC+S6 composites to response to the electric field to some extent.

4. CONCLUSIONS

To address the problem of CNT aggregations and further expand the potential applications of CNTs in the field of functional materials, a series of novel CNSs are prepared to disperse CNTs. CNSs with more mole fraction of polycyclic conjugated structure have better ability to load and disperse CNTs. The evenly dispersed CNTs can lower the glass transition temperature, strengthen the thermal stability because of the interaction between CNSs and CNTs, decrease the thermochromic temperature by bringing anisotropic thermal conductivity to the helical matrix of CNSs and enrich the reflected colors of CNSs. To apply the CNSs to disperse CNTs in chiral host and to promote the compatibility between CNTs and chiral host, a ternary chiral system is established by CLCs, S6, and CNTs. CNTs are effectively dispersed in CLC host by surfactant S6, and the CNT dispersed CLCs exhibit a faster electro-optical response process than neat CLCs. We believe that the above-reported win-win strategy will be a promising mode for researchers to address the dispersion of CNTs and to apply CNTs to improve the thermal, optical, and electro-optical properties of dispersion medium.

■ ASSOCIATED CONTENT

Supporting Information

Synthesis of CNSs, optical textures of L581, converting RGB values to chromaticity coordinates, RGB values, tristimulus values, and chromaticity coordinates of S6, S6 + 0.4%CNT and S6 + 0.7%CNT at different temperatures. This material is available free of charge via the Internet at http://pubs.acs.org.

■ AUTHOR INFORMATION

Corresponding Author

*Tel: +86 024-83687446. E-mail: baoyanzhang@hotmail.com.

Notes

The authors declare no competing financial interest.

■ ACKNOWLEDGMENTS

The authors are grateful to National Basic Research Priorities Program of China, Educational Science and Technology Program of Liaoning Province, and the Science and Technology Department of Liaoning Province for support of this work.

■ REFERENCES

(1) Iijima, S. Helical Microtubules of Graphitic Carbon. *Nature* **1991**, *354*, 56−58.

(2) Chen, Z.; Yuan, Y.; Zhou, H.; Wang, X.; Gan, Z.; Wang, F.; Lu, Y. 3D Nanocomposite Architectures from Carbon-Nanotube-Threaded Nanocrystals for High-Performance Electrochemical Energy Storage. *Adv. Mater.* **2014**, *26*, 339−345.

(3) Chen, H.; Kang, Y.; Cai, F.; Zeng, S.; Li, W.; Chen, M.; Li, Q. Electrochemical Conversion of $Ni_2(OH)_2CO_3$ into $Ni(OH)_2$ Hierarchical Nanostructures Loaded on a Carbon Nanotube Paper with High Electrochemical Energy Storage Performance. *J. Mater. Chem. A* **2015**, *3*, 1875−1878.

(4) Liu, P.; Wei, Y.; Liu, K.; Liu, L.; Jiang, K.; Fan, S. New-Type Planar Field Emission Display with Superaligned Carbon Nanotube Yarn Emitter. *Nano Lett.* **2012**, *12*, 2391−2396.

(5) Vasilyeva, S. V.; Unur, E.; Walczak, R. M.; Donoghue, E. P.; Rinzler, A. G.; Reynolds, J. R. Color Purity in Polymer Electrochromic Window Devices on Indium-Tin Oxide and Single-Walled Carbon Nanotube Electrodes. *ACS Appl. Mater. Interfaces* **2009**, *10*, 2288−2297.

(6) Peng, L. M.; Zhang, Z.; Wang, S. Carbon Nanotube Electronics: Recent Advances. *Mater. Today.* **2014**, *17*, 433−442.

(7) Jin, S. H.; Shin, J.; Cho, I. T.; Han, S. Y.; Lee, D. J.; Lee, C. H.; Lee, J. H.; Rogers, J. A. Solution-Processed Single-Walled Carbon Nanotube Field Effect Transistors and Bootstrapped Inverters for Disintegratable, Transient Electronics. *Appl. Phys. Lett.* **2014**, *105*, No. 013506.

(8) Kim, J. H.; Heller, D. A.; Jin, H.; Barone, P. W.; Song, C.; Zhang, J.; Trudel, L. J.; Wogan, J. N.; Tannenbaum, S. R.; Strano, M. S. The Rational Design of Nitric Oxide Selectivity in Single-Walled Carbon Nanotube Near-Infrared Fluorescence Sensors for Biological Detection. *Nat. Chem.* **2009**, *1*, 473−481.

(9) Fan, J. C.; Shi, Z. X.; Tian, M.; Wang, J. L.; Yin, J. Unzipped Multiwalled Carbon Nanotube Oxide/Multiwalled Carbon Nanotube Hybrids for Polymer Reinforcement. *ACS Appl. Mater. Interfaces* **2012**, *4*, 5956−5965.

(10) Liu, Y. D.; Kumar, S. Polymer/Carbon Nanotube Nano Composite Fibers—A Review. *ACS Appl. Mater. Interfaces* **2014**, *6*, 6069−6087.

(11) Wang, D.; Ji, W. X.; Li, Z. C.; Chen, L. W. A Biomimetic "Polysoap" for Single-Walled Carbon Nanotube Dispersion. *J. Am. Chem. Soc.* **2006**, *128*, 6556−6557.

(12) Pénicaud, A.; Dragin, F.; Pécastaings, G.; He, M.; Anglaret, E. Concentrated Solutions of Individualized Single Walled Carbon Nanotubes. *Carbon* **2014**, *67*, 360−367.

(13) Bravo-Sanchez, M.; Simmons, T. J.; Vidal, M. A. Liquid Crystal Behavior of Single Wall Carbon Nanotubes. *Carbon* **2010**, *48*, 3531−3542.

(14) Lagerwall, J. P. F.; Scalia, G. Carbon Nanotubes in Liquid Crystals. *J. Mater. Chem.* **2008**, *18*, 2890−2898.

(15) Ma, J.; Larsen, R. M. Comparative Study on Dispersion and Interfacial Properties of Single Walled Carbon Nanotube/Polymer Composites Using Hansen Solubility Parameters. *ACS Appl. Mater. Interfaces* **2013**, *5*, 1287−1293.

(16) Goak, J. C.; Lee, S. H.; Han, J. H.; Jang, S. H.; Kim, K. B.; Seo, Y. H.; Seo, Y. S.; Lee, N. Spectroscopic Studies and Electrical Properties of Transparent Conductive Films Fabricated by Using Surfactant-Stabilized Single-Walled Carbon Nanotube Suspensions. *Carbon* **2011**, *49*, 4301−4313.

(17) Zhong, W.; Claverie, J. P. Probing the Carbon Nanotube-Surfactant Interaction for the Preparation of Composites. *Carbon* **2013**, *51*, 72−84.

(18) Nie, M.; Kalyon, D. M.; Fisher, F. T. Interfacial Load Transfer in Polymer/Carbon Nanotube Nanocomposites with a Nanohybrid Shish Kebab Modification. *ACS Appl. Mater. Interfaces* **2014**, *6*, 14886−14893.

(19) Petrie, K.; Docoslis, A.; Vasic, S.; Kontopoulou, M.; Morgan, S.; Ye, Z. B. Non-Covalent/Non-Specific Functionalization of Multi-Walled Carbon Nanotubes with a Hyperbranched Polyetylene and Characterization of their Dispersion in a Polyolefin Matrix. *Carbon* **2011**, *49*, 3378−3382.

DOI: 10.1021/acsami.5b00168
ACS Appl. Mater. Interfaces 2015, 7, 6724−6732

(20) Badaire, S.; Zakri, C.; Maugey, M.; Derré, A.; Barisci, J. N.; Wallace, G.; Poulin, P. Liquid Crystals of DNA-Stabilized Carbon Nanotubes. *Adv. Mater.* **2005**, *17*, 1673−1676.
(21) Nakashima, N. Solubilization of Single-Walled Carbon Nanotubes with Condensed Aromatic Compounds. *Sci. Technol. Adv. Mater.* **2006**, *7*, 609−616.
(22) Dierking, I.; Scalia, G.; Morales, P. Liquid Crystal-Carbon Nanotube Dispersions. *J. Appl. Phys.* **2005**, *97*, No. 044309.
(23) Kim, J. Y.; Kim, D. K.; Kim, S. H. Effect of Modified Carbon Nanotube on Physical Properties of Thermotropic Liquid Crystal Polyester Nanocomposites. *Eur. Polym. J.* **2009**, *45*, 316−324.
(24) Basu, R.; Iannacchione, G. S. Nematic Anchoring on Carbon Nanotubes. *Appl. Phys. Lett.* **2009**, *95*, No. 173113.
(25) Chen, H. Y.; Lee, W. Electro-Optical Characteristics of a Twisted Nematic Liquid-Crystal Cell Doped with Carbon Nanotubes in a DC Electric Field. *Opt. Rev.* **2005**, *12*, 223−225.
(26) Chen, H. Y.; Lee, W.; Clark, N. A. Faster Electro-Optical Response Characteristics of a Carbonnanotube-Nematic Suspension. *Appl. Phys. Lett.* **2007**, *90*, No. 033510.
(27) Islam, M. F.; Alsayed, A. M.; Dogic, Z.; Zhang, J.; Lubensky, T. C.; Yodh, A. G. Nematic Nanotube Gels. *Phys. Rev. Lett.* **2004**, *92*, No. 088303.
(28) Lee, H. W.; You, W.; Barman, S.; Hellstrom, S.; LeMieux, M. C.; Oh, J. H.; Liu, S. H.; Fujiwara, K.; Wang, W. C. M.; Chen, B.; Jin, Y. W.; Kim, J. M.; Bao, Z. Lyotropic Liquid-Crystalline Solutions of High-Concentration Dispersions of Single-Walled Carbon Nanotubes with Conjugated Polymers. *Small* **2009**, *5*, 1019−1024.
(29) Basu, R.; Iannacchione, G. Orientational Coupling Enhancement in a Carbon Nanotube Dispersed Liquid Crystal. *Phys. Rev. E* **2010**, *81*, No. 051705.
(30) Prasad, S. K.; Kumar, M. V.; Yelamaggad, C. V. Dual Frequency Conductivity Switching in a Carbon Nanotube/Liquid Crystal Composite. *Carbon* **2013**, *59*, 512−517.
(31) Ji, Y.; Huang, Y. Y.; Terentjev, E. M. Dissolving and Aligning Carbon Nanotubes in Thermotropic Liquid Crystals. *Langmuir* **2011**, *27*, 13254−13260.
(32) Jeong, H. S.; Ko, Y. K.; Kim, Y. H.; Yoon, D. K.; Jung, H. T. Self Assembled Plate-Like Structures of Single-Walled Carbon Nanotubes by Non-Covalent Hybridization with Smectic Liquid Crystals. *Carbon* **2010**, *48*, 774−780.
(33) Hsu, S. H.; Wu, M. C.; Chen, S.; Chuang, C. M.; Lin, S. H.; Su, W. F. Synthesis, Morphology and Physical Properties of Multi-Walled Carbon Nanotube/Biphenyl Liquid Crystalline Epoxy Composites. *Carbon* **2012**, *50*, 896−905.
(34) Jian, B. R.; Tang, C. Y.; Lee, W. Temperature-Dependent Electrical Properties of Dilute Suspensions of Carbon Nanotubes in Nematic Liquid Crystals. *Carbon* **2011**, *49*, 910−914.
(35) Xiong, J. W.; Zheng, Z.; Qin, X. M.; Li, M.; Li, H. Q.; Wang, X. L. The Thermal and Mechanical Properties of a Polyurethane/Multi-Walled Carbon Nanotube Composite. *Carbon* **2006**, *44*, 2701−2707.
(36) Kim, J. Y. Carbon Nanotube-Reinforced Thermotropic Liquid Crystal Polymer Nanocomposites. *Materials* **2009**, *2*, 1955−1974.
(37) Woon, K. L.; O'Neill, M.; Dessaud, N. Stokes Parameter Studies of Spontaneous Emission from Chiral Nematic Liquid Crystals as a One-Dimensional Photonic Stopband Crystal: Experiment and Theory. *Phys. Rev. E* **2005**, *71*, No. 041706.
(38) San Jose, B. A.; Yan, J. L.; Akagi, K. Dynamic Switching of the Circularly Polarized Luminescence of Disubstituted Polyacetylene by Selective Transmission through a Thermotropic Chiral Nematic Liquid Crystal. *Angew. Chem.* **2014**, *126*, 10817−10820.
(39) Bisoy, H. K.; Li, Q. Light-Directing Chiral Liquid Crystal Nanostructures: From 1D to 3D. *Acc. Chem. Res.* **2014**, *47*, 3184−3195.
(40) Mitov, M. Cholesteric Liquid Crystals with a Broad Light Reflection Band. *Adv. Mater.* **2012**, *24*, 6260−6276.
(41) Blinov, L. M.; Palto, S. P. Cholesteric Helix: Topological Problem, Photonics and Electro-Optics. *Liq. Cryst.* **2009**, *36*, 1037−1047.

DOI: 10.1021/acsami.5b00168
ACS Appl. Mater. Interfaces 2015, 7, 6724−6732